NAMPT inhibition suppresses cancer stem-like cells associated with therapy-induced senescence in ovarian cancer

Timothy Nacarelli [1 #], Takeshi Fukumoto [1 #], Joseph A. Zundell [1], Nail Fatkhutdinov [1], Stephanie Jean [2], Mark G. Cadungog [2], Mark E. Borowsky [2], Rugang Zhang[1] *

[1] Gene Expression and Regulation Program, The Wistar Institute, Philadelphia, PA 19104, USA

[2] Helen F. Graham Cancer Center & Research Institute, Newark, DE 19713

* Correspondence should be addressed to:

Rugang Zhang, Ph.D.

Gene Expression and Regulation Program, The Wistar Institute

3601 Spruce Street, Philadelphia, PA 19104

Phone: 215-495-6840

E-mail: rzhang@wistar.org

[#] T.Nacarelli and T. Fukumoto contributed equally to this article.

Running title: NAMPT inhibition and Senescence-Associated Stemness

Disclosure of Potential Conflicts of Interests: The authors declare no competing financial interests.

Abstract

Epithelial ovarian cancer (EOC) is the most lethal of gynecologic malignancies. The standard-of-care treatment for EOC is platinum-based chemotherapy such as cisplatin. Platinum-based chemotherapy induces cellular senescence. Notably, therapy-induced senescence contributes to chemoresistance by inducing cancer stem-like cells (CSCs). However, therapeutic approaches targeting senescence-associated CSCs remain to be explored. Here, we show that NAMPT inhibition suppresses senescence-associated CSCs induced by platinum-based chemotherapy in EOC. Clinically applicable NAMPT inhibitors suppressed the outgrowth of cisplatin-treated EOC cells both *in vitro* and *in vivo*. Moreover, a combination of the NAMPT inhibitor FK866 and cisplatin improved the survival of EOC-bearing mice. These phenotypes correlated with inhibition of the CSCs signature, which consists of elevated expression of ALDH1A1 and stem-related genes, high ALDH activity, and CD133 positivity. Mechanistically, NAMPT regulates EOC CSCs in a paracrine manner through the senescence-associated secretory phenotype. Our results suggest that targeting NAMPT using clinically applicable NAMPT inhibitors, such as FK866, in conjunction with platinum-based chemotherapy represents a promising therapeutic strategy by suppressing therapy-induced senescence-associated CSCs.

Statement of Significance

This study highlights the importance of NAMPT-mediated NAD^+ biosynthesis in the production of cisplatin-induced senescence-associated cancer stem cells, as well as tumor relapse after cisplatin treatment.

Introduction

More than 85% of ovarian cancers are of epithelial origin (1). Epithelial ovarian cancer (EOC) is broadly divided into 2 types (1). Type I EOC includes endometrioid, mucinous, low-grade serous, and clear cell carcinomas, while type II EOC includes high-grade serous carcinomas (HGSC) (1). Platinum-based chemoresistance is a major obstacle in the clinical management of EOC. EOC, in particular type II HGSC, initially respond well to platinum-based chemotherapy such as cisplatin, but the majority of these cases relapse with fatal chemoresistant EOC (2). For example, up to 80% of women with advanced stage type II HGSC experience recurrence after first-line chemotherapy (1). Accumulating evidence indicates that a key contributor of EOC chemoresistance is cancer stem-like cells (CSCs), which are a subpopulation of chemoresistant cancer cells with stem-like properties (3). EOC CSCs are chiefly characterized by the stem cell surface marker CD133 and elevated aldehyde dehydrogenase 1 (ALDH1) activity mainly through the upregulation of ALDH1A1. Positivity for CD133 and ALDH1 CSC markers in EOC patient tumor samples predict a worse outcome (4-6). Indeed, inhibition of ALDH activity is sufficient to sensitize EOC cells to chemotherapy (7). Consistently, ALDH activity is also increased in a population of cancer-prone normal ovarian stem cells (8). However, clinically applicable approaches to eliminate EOC CSCs remain to be developed.

Platinum-based chemotherapies, such as cisplatin and carboplatin, are known to induce cellular senescence (2,9). Cellular senescence is an essential tumor suppressive mechanism that limits the propagation of cells subjected to insults such as chemotherapeutics (10). In this case, cells undergo therapy-induced senescence. Interestingly, therapy-induced senescent cells can spontaneously escape from the arrested condition and cells released from senescence re-entered the cell cycle with a much higher tumor initiation potential (11). Senescent cells

maintain viability and undergo a stable proliferative arrest associated with a series of phenotypic changes. A key phenotypic change is the acquisition of a secretory phenotype known as the senescence-associated secretory phenotype (SASP). The SASP consists of a plethora of secreted factors including cytokines and chemokines, such as IL6, IL8, and IL1B. Ironically, the SASP has paracrine effects that are pro-tumorigenic, and emerging evidence supports the role of the SASP in the induction of cancer stemness and relapse (12-14). Additionally, evidence shows that selectively eliminating senescent cells suppresses cancer stemness following chemotherapy treatment (15). However, directly eliminating senescent cells as a cancer therapy approach may be associated with unintended side-effects (11,15). Thus, an ideal therapeutic strategy is to eliminate the induction of senescence-induced CSCs through targeting the SASP, while not affecting the tumor suppressive proliferative arrest of senescent cells.

Nicotinamide phosphoribosyltransferase (NAMPT) is the rate-limiting enzyme for the NAD^+ biosynthetic salvage pathway (16). NAD^+ plays a critical pathophysiological role in tissue aging and cancer development (17). For instance, the NAMPT pathway becomes deficient during tissue aging and supplementation with NAD^+ precursors, such as nicotinamide mononucleotide (NMN), which have been employed as a preventative anti-aging strategy (18). However, the NAMPT pathway is overexpressed and has been explored as a therapeutic target in multiple types of cancer, where clinically applicable inhibitors such as FK866 and GMX1778 have been developed (19,20). Notably, NAMPT drives activation of the SASP through the NFκB-dependent pathway and promotes tumorigenesis (21). Indeed, pharmacological inhibition of NAMPT suppressed the SASP while enhancing the tumor suppressive senescence-associated proliferative arrest (21). Thus, NAMPT represents an ideal target to selectively eliminate the tumor-promoting SASP, while enhancing the tumor suppressive senescence-associated growth arrest. However, its role in senescence-associated CSCs induced by chemotherapy has not previously been investigated.

Here we show that the NAMPT-regulated NAD^+ biosynthetic pathway mediates senescence-associated CSCs in EOC following platinum-based chemotherapy in a paracrine manner through promoting the SASP. The combination of cisplatin treatment with pharmacological inhibition of NAMPT suppresses the EOC CSC signature. This correlates with a suppression of the outgrowth of cisplatin-treated EOC cells both *in vitro* and *in vivo* and an improvement of the survival of EOC-bearing mice in a xenograft model.

Materials and Methods

Cell lines and culture conditions

The EOC cell lines OVCAR3 and OVCAR5 were cultured in RPMI 1640 (Corning) supplemented with 10% fetal bovine serum (Sigma-Aldrich) and 1% penicillin/streptomycin. All cell lines were obtained from ATCC and reauthenticated by The Wistar Institute Genomics Facility using short tandem repeat profiling using AmpFLSTR Identifiler PCR Ampliciation Kit (Life Technologies). We performed mycoplasma testing using LookOut Mycoplasma PCR detection (Sigma) every month.

Reagents and antibodies

The following antibodies were purchased from the indicated supplied and used for immunoblotting: Rabbit monoclonal anti-HMGA1 (Sigma, cat. no. 129153), rabbit polyclonal anti-NAMPT (Bethyl Laboratories, cat. no. A300-372A), mouse monoclonal anti-β-Actin (Sigma, cat. no. 2532), ALDH1 (BD laboratories, cat. no. 611195), rabbit polyclonal anti-Lamin B1 (Abcam, cat. no. ab65986), cleaved PARP1 (Promega, cat. no. G7341), cleaved caspase 3 (Cell Signaling, cat. no. 9662). The following compounds were purchased from the indicated suppliers and used at the indicated concentrations for *in vitro* studies: cisplatin (Selleck, cat. no. S1166), 250 nM; carboplatin (Selleck, cat. no. S1215), 500 nM; FK866 (Millipore, cat. no. 48-190-82), 1 nM; GMX1778 (Selleck, cat. no. S8117), 0.5 nM; NMN (Sigma, cat. no. N3501), 500 μM; and doxycycline (Selleck, cat. no. S4163), 1 μg/ml.

Quantitative reverse-transcriptase PCR (qRT-PCR)

We performed qRT-PCR following RNA extraction using TRIzol (Thermo Fisher) and DNase treatment (RNeasy columns by Qiagen). RNA expression was measured using an iTaq Universal SYBR Green One-step kit (Bio-Rad Laboratories) on a QuantStudio 3 Real-Time PCR

machine (Thermo Fisher). For human genes, β2-microglobulin (*B2M*) was used as an internal control. For mouse genes, cyclophilin A was used as an internal control. The fold change was calculated using the $2^{-\Delta C(t)}$ method for all analyses. Primer sequences for the indicated genes are as follows: *IL1B* (forward: AGCTCGCCAGTGAAATGATGG, reverse: GTCCTGGAAGGAGCACTTCAT); *IL6* (forward: ACATCCTCGACGGCA TCTCA; reverse: TCACCAGGCAAGTCTCCTCA); *IL8* (forward: GCTCTGTGTGAAGGTGCAGT; reverse: TGCACCCAGTTTTCCTTGGG); *ALDH1A1* (forward: AGCAGGAGTGTTTACCAAAGA; reverse: CCCAGTTCTCTTCCATTTCCAG); *SOX2* (forward: GGAGGGGTGCAAAAGAGGAGAG; reverse: TCCCCCAAAAAGAAGTCCAGG); *NESTIN1* (forward: GGGAGTTCTCAGCCTCCAG; reverse: GGAGAAACAGGGCCTACAGA); *LRIG1* (forward: GGTGAGCCTGGCCTTATGTGAATA; reverse: CACCACCATCCTGCACCTCC); *LGR5* (forward: GACTTTAACTGGAGCACAGA; reverse: AGCTTTATTAGGGATGGCAA); *CD133* (forward: GGGTGTATCCAAAACCCGGA; reverse: ACACTGAAAGTTACATCCACAGAA); *CD44* (forward: GCAGGTATGGGTTCATAGAAGG; reverse: GGTGTTGGATGTGAGGATGT), mouse *ALDH1A1* (forward: CGCAAGACAGGCTTTTCAG; reverse: TGTATAATAGTCGCCCCCTCTC); mouse *IL6* (forward: GCTACCAAACTGGATATAATCAGGA; reverse: CCAGGTAGCTATGGTACTCCAGAA); and mouse *CYCLOPHILIN A* (forward: GGGTTCCTCCTTTCACAGAA; reverse: GATGCCAGGACCTGTATGCT).

Chromatin immunoprecipitation (ChIP)

ChIP analysis was performed as previously described (21). Specifically, cells were fixed for 5 min at room temperature using 1% formaldehyde (Thermo Fisher) and then incubated for an additional 5 min at room temperature with 2.5 M glycine. Then, cells were washed twice using cold PBS and then lysed using ChIP lysis buffer (50 mM HEPES-KOH (pH 7.5), 1 mM EDTA

(pH 8.0), 140 mM NaCl, 1% Triton X-100 and 0.1% deoxycholate with 0.1 mM PMSF and EDTA-free Protease Inhibitor Cocktail). After incubation on ice for 10 min, the lysed samples were centrifuged at 3,000 rpm. for 3 min at 4 °C. The resulting pellet was resuspended in a second lysis buffer (10 mM Tris (pH 8.0), 1 mM EDTA, 200 mM NaCl and 0.5 mM EGTA with 0.1 mM PMSF and EDTA-free Protease Inhibitor Cocktail) and incubated at room temperature for 10 min before centrifugation at 3,000 rpm for 5 min at 4 °C. Next, the pellet was resuspended in a third lysis buffer (100 mM NaCl, 10 mM Tris (pH 8.0), 1 mM EDTA, 0.1% doxycycline (DOX), 0.5 mM EGTA and 0.5% *N*-lauroylsarcosine with 0.1 mM PMSF and EDTA-free Protease Inhibitor Cocktail) and sonicated using a Biorupter (Diagenode) for 15 min (30s on and 1min off). Each ChIP sample received 10% Triton X-100 and was centrifuged at maximum speed for 15 min at 4 °C. The supernatant of each ChIP sample was collected for quantification of DNA and precleared using 15 µl of protein G Dynabeads (Thermo Fisher) for 1 hour at 4 °C. The samples were centrifuged at maximum speed for 15 min at 4 °C and then the supernatant of each sample was incubated with 50 µl of antibody-bead conjugate solution for immunoprecipitation overnight on a rotator at 4 °C. The following day, each sample was washed on a rotator for 15 min at 4 °C using ChIP lysis buffer containing 0.65 M NaCl, wash buffer (250 mM LiCl, 10 mM Tris-HCl (pH 8.0), 0.5% DOC, 0.5% NP-30 and 1 mM EDTA (pH 8.0)), and TE buffer (1 mM EDTA (pH 8.0) and 10 mM Tris-HCl (pH 8.0)). Then, DNA was eluted by incubation of the beads with TE buffer + 1% SDS for 15 min at 65 °C. Subsequently, the samples were then incubated overnight at 65 °C to reverse crosslinking. The next day, the samples were incubated in proteinase K (1 mg/ml) for 5 hours at 37 °C. Then, the DNA was purified from each sample using a Wizard SV Gel and PCR Clean Up kit (Promega). We performed quantitative PCR on the immunoprecipitated DNA using iTaq Universal SYBR Green (Bio-Rad Laboratories) using primers for the *NAMPT* enhancer site (forward:

GAGTGAGGCCTGCACAAGTA; reverse: TCTCAGGCAAATGGTGATTG). Isotype-matched IgG served as a negative control.

Colony formation

Cells were cultured in 24-well plates (1,000 cells per well) for one to two weeks based on the experiment. Colonies were washed twice with PBS and fixed with 10% acetic acid and 10% methanol in distilled water. Plates were stained using 0.05% crystal violet for visualization. Analysis was performed based on integrated density using NIH ImageJ Software.

NAD^+/NADH ratio

The NAD^+/NADH ratio was measured using the NAD/NADH-Glo Assay (Promega, G9071) based on the manufacturer's instructions. Luminescence signals were measured using a Victor X3 2030 Multilabel Reader (Perkin Elmer).

Immunoblotting

Cells were lysed using 1X sample buffer (10% glycerol, 2% SDS, 0.01% bromophenol blue, 0.1 M dithiothreitol (DTT) and 62.5 mM Tris buffer (pH 6.8) to isolate protein. The cell lysate was heated at 95 °C for 10 min and the protein extract concentration was determined using the Bradford assay. An equal protein concentration was used for SDS–PAGE and transferred to a nitrocellulose membrane at 100 V for 2 hours at 4 °C. Then, the membrane was blocked using 5% nonfat milk in TBS/0.1% Tween 20 (TBST) for 1 hour at room temperature. The membrane was incubated with primary antibodies of interest overnight at 4 °C in 4% BSA/TBS + 0.025% sodium azide. The next day, the membrane was washed with TBST for 5 min at room temperature three times and then incubated with horseradish peroxidase- conjugated secondary antibodies (Cell Signaling Technology) made up in 5% nonfat milk for 1 hour at room temperature. Then, the membrane was washed with TBST for 5 min at room temperature 3

times and incubated with SuperSignal West Pico PLUS Chemiluminescent Substrate (Thermo Fisher) for visualization by film.

Flow cytometry

ALDH activity was measured using the Aldefluor assay kit (Stem Cell Technologies, cat. no. 1700) based on the manufacturer's instructions. Cells were resuspended in Aldefluor assay buffer with the ALDH substrate for 30 min at 37 °C. Then, cells were washed in PBS and incubated with an anti-CD133-PE/Cy7 antibody (Biolegend, cat. no. 372810) in Aldefluor assay buffer for 20 min on ice. Then, cells were washed and resuspended in PBS and submitted for analysis. Samples were run on an LSR-II flow cytometer (Becton Dickinson). For the detection of ALDH and SA-β-Gal activity, unfixed cells were stained with AldeRed (Millipore Sigma, cat. no. SCR150) for 30 min at 37 °C in Aldefluor assay buffer, washed in PBS, and then stained with SPiDER-β-Gal (Dojindo Technologies, cat. no. SG02-10) in Aldefluor assay buffer at the pH of 7.2 for 20 min at 37 °C. Cells were run and sorted using an Aria-II flow cytometer (Becton Dickinson). Flow cytometric Annexin V and propidium iodide staining (Thermo Fisher, cat. no. V13242) was used to detect apoptosis following the manufacturer's instructions. Briefly, cells were trypsinized, washed with cold PBS, and stained with annexin V and propidium iodide at room temperature followed by analysis. All data was analyzed using FlowJo version 7 software. For the analysis of mouse tumors, tumors were extracted using the mouse tumor dissociation kit (Miltenyi Biotech, cat. no. 130-096-730) based on the manufacturer's instructions. Following dissociation, the cells were filtered through a 40 μM cell strainer before preceding to staining.

Sphere formation assay

Cells were stained for ALDH and SA-β-Gal activity using the aforementioned method and sorted based on double positive or negative staining. The sorted cells were cultured in ultra-low attachment plates (Corning, cat no. CLS3473) in a serum-free mammary epithelial growth

medium (Lonza, cat. no. CC3150) supplemented with B27 (Life Technologies, cat. no. 17504044), 20 ng/mL EGF (Invitrogen, cat. no. PHG0311), and 20 ng/mL FGF (Peprotech, cat. no. AF-100-26). The sorted cells were cultured in medium with or without 1 nM FK866, 0.5 nM GM1778, or 500 μM NMN. Spheres larger than 50 μm were quantified seven days later.

Organoid-like cultures

The procurement of human ovarian tumor tissues was approved by the Institutional Review Board of Christina Care Health System. De-identified patient tumor samples were obtained from Helen F. Graham Cancer Center at Christiana Care Health System. The tumor sample was processed into single cells by mincing using a scalpel, incubation with Type II Collagenase (Life Technologies, cat. no. 17101015) at 37 °C for 10 minutes, and then incubation with trypsin-EDTA (Corning, cat. no. 25-053CI) + 50 U/mL DNase (Qiagen, cat. no. 79454) at 37 °C for 10 minutes. The tumor sample was centrifuged at 3000 rpm for 3 minutes and the supernatant was collected and filtered through a 40 μm strainer to isolate single cells. This step was repeated to ensure the isolation of single cells. The sample was centrifuged at 3000 rpm for 3 minutes and resuspended in Basal culture media for enumeration by hemocytometry. Next, 5,000 cells were mixed with 100 μl of growth factor-reduced matrigel (Corning, cat. no. CB-40230C) and seeded as a 100 μl droplet in a 24 well plate. After the matrices in the wells solidified, 500 μl of organoid media was added. Media was refreshed every other day and organoids were passaged every two weeks. Basal culture media consisted of Advanced DMEM/F12 (Thermo Fisher, cat. no. 10-092CM), 1X Glutamax (Thermo Fisher, cat. no. 35050061), and 1% HEPES (Life Technologies, cat. no. 15630080). Organoid media consisted of basal culture media supplemented with 1X N2 (Invitrogen, cat. no. 17502048), 1X B27 (Invitrogen, cat. no. 17504044), 0.5 M N-acetylcysteine (Sigma, cat. no. A7250), 5 mM CHIR-99021 (Selleck, cat. no. S2924), 500 μg/ml EGF (Peprotech, cat. no. 100-15), 500 nM A83-01 (Sigma, cat. no. SML0788), 1 μM SB202190

(Sigma, cat. no. S7067), 100 nM Gastrin (Sigma, cat. no. G9020), 4 mM nicotinamide (Sigma, cat. no. 47865), 10 μM Y27632 (Selleck, S1049), 1X anti-anti (Sigma, cat. no. A5955-20), 100 ng/ml FGF10 (Peprotech, cat. no. AF-100-26), and WNR conditioned media (containing Noggin/R-Spondin/Wnt3a). The organoid-like culture was imaged using phase-contrast microscopy and on a Celígo imaging cytometer (Nexcelom) following staining using Aldefluor at 37 °C for 30 minutes. This system was not compatible with staining for CD133. For analysis, we quantified organoids larger than 40 μm. For hematoxylin and eosin histological staining, the organoids were fixed using 4% paraformaldehyde (Sigma, cat. no. 158127) and washed with PBS before resuspension in embedding matrix consisting of 2% bacto-agar (BD laboratories, cat. no. DF0140-15-4) + 2% gelatin (Sigma, 9000-70-8). After solidification, the organoids were placed in a histo-cassette for histological processing.

Lentivirus production and infection

To generate the doxycycline-inducible knockdown NAMPT construct, we cloned the short hairpin RNA (shRNA) sequence against NAMPT into a tet-pLKO-puro plasmid (Addgene, cat. no. 21915). The short hairpin RNA (shRNA) against NAMPT was obtained from the Molecular Screening Facility at the Wistar Institute: TRCN0000116177, sense sequence: CCACCTTATCTTAGAGTTATT. For inducing knockdown of NAMPT, the cells were treated with 1 μg/mL of doxycycline for at least 72 hours. Lentivrius was produce using the ViraPower kit (Invitrogen, cat. no. K4975-00) based on the manufacturer's instructions using the 293FT human embryonic kidney cell line. EOC cells infected with viruses encoding the puromycin resistance gene were selected using 3 μg/mL of puromycin.

SA-β-Gal staining

Cells were fixed using 2% formaldehyde/0.2% glutaraldehyde in PBS and washed twice with PBS. Cells were then incubated in an X-Gal solution (150 mM NaCl, 2 mM $MgCl_2$, 5 mM $K_3Fe(CN)_6$, 5 mM $K_4Fe(CN)_6$, 40 mM Na_2HPO_4 (pH 6.0), and 1 mg ml^{-1} X-gal) overnight at 37 °C in a non-CO_2 incubator. SA-β-Gal staining was performed at the pH of 5.7 to enhance sensitivity of detection. Cells were enumerated based on the percentage of SA-β-Gal positive cells.

NFκB Reporter Assay

NFκB activity was measured using the NFκB reporter plasmid (Addgene, plasmid no. 49343) and readout data was normalized based on the transfection efficiency of the pRL-SV40 plasmid renilla luciferase (Addgene, plasmid no. E223A). Lipofectamine 3000 Reagent (Invitrogen) was used for plasmid co-transfection and cells were assayed for luminescence using a Dual-Luciferase Reporter Assay System (Promega, cat no. E1910). Luminescence was measured using a Victor X3 2030 Multilabel Reader (Perkin Elmer).

Animal experiments

All animal protocols described in this study were approved by the Wistar Institutional Animal Care and Use Committee (IACUC). The subcutaneous tumor xenograft models and the measurement of tumor size were performed as previously described (22). Briefly, $9x10^6$ OVCAR3 cells were suspended in 100 μL solution (PBS : Matrigel =1:1) and injected subcutaneously into the right dorsal flank of 6-8 week-old female immunocompromised non-obese diabetic/severe combined immunodeficiency gamma (NSG) mice. Notably, $9x10^6$ OVCAR3 cells produced the most reproducible result of developing palpable tumors within 4 weeks. Tumors were allowed to establish until the tumor size was palpable, and then the mice were randomly assigned to be treated for three weeks with vehicle controls, FK866 (10 mg/kg

i.p. once-a-day), cisplatin (750 μg/kg i.p. twice, once every two weeks) or a combination of the two compounds. The doses of compounds were determined based on previous studies (23-25). FK866 was suspended in 45% Propylene glycol+5% Tween 80 +ddH^2O, and cisplatin was suspended in PBS. Tumor size was measured twice-a-week by two investigators as follows: tumor size (mm^3) = [d^2 x D]/2, d is the shortest diameter and D is the largest diameter. After three weeks of treatments, tumors samples were surgically dissected from half number of mice of each group, and the tumor weights were measured as a surrogate for tumor burden. The other half of the mice cohort of each group were followed for the survival experiment. The Wistar IACUC guideline was followed in evaluating the survival of tumor-bearing mice.

Immunohistochemical staining

Immunohistochemical staining was performed on the consecutive sections from xenografted tumors dissected from NSG mice treated with vehicle controls, FK866 (10 mg/kg i.p. once-a-day), cisplatin (750 μg/kg i.p. twice, once every two weeks) or a combination of the two compounds. The tumor samples were fixed in 10% buffered formalin and embedded in paraffin. The sections cut from paraffin embedded blocks were deparaffinized with xylene and ethanol, and then immersed for 40 min in 10mM citric acid buffer, pH 6.0. The activity of endogenous peroxides was quenched for 20 min in 3% H_2O_2 in methanol. After rinsing in PBS, the sections were incubated at 4 °C with anti-ALDH1 antibody overnight. Then, Dako EnVision+ system was conducted following the manufacturer's instructions. Finally, the sections were counterstained with Mayer's hematoxylin (Sigma). Expression of ALDH1 stains of each group was scored using a histologic score (H-score) by two investigators.

Database mining

Database mining of the Cancer Genome Atlas (TCGA) ovarian cancer transcriptome dataset was performed using the publically-available Gene Expression Profiling Interactive Analysis software (26). Database mining was also conducted on a clinically annotated microarray dataset that is publicly available in the Gene Expression Omnibus (GSE9891) (27). Analysis was conducted by sorting 267 EOC tumors based on low and high *NAMPT* expression and analyzed for the expression of *IL6*, *IL1B*, and *IL8*. The mean of *NAMPT* expression was determined and samples below the mean were considered low *NAMPT* expressing and samples above the mean were considered high *NAMPT* expressing.

Statistical analysis and reproducibility

Results are representative of a minimum of three independent experiments unless otherwise stated. All quantitative data are expressed as mean ± S.E.M. Statistical analyses were conducted using GraphPad Prism 6 (GraphPad). A Student's *t*-test was performed to determine *P* values where $P<0.05$ was considered statistically significant.

Results

NAMPT inhibition suppresses the SASP during platinum-induced senescence

HMGA1 is a key regulator of *NAMPT* expression during cellular senescence (21). NAMPT is the rate-limiting enzyme for the NAD^+ salvage pathway and plays a key role in activation of the SASP (21). Thus, we sought to examine if HMGA1-mediated upregulation of NAMPT promotes the SASP following platinum-induced senescence in EOC cells. Indeed, HMGA1 was upregulated and bound to the *NAMPT* gene enhancer by chromatin immunoprecipitation (ChIP) analysis in cisplatin-induced senescent OVCAR3 cells (**Figure 1A-B**). Consistently, NAMPT expression and the NAD^+/NADH ratio were significantly elevated in the senescent cells (**Figure 1B-C**). Inhibition of NAMPT activity using the small-molecule inhibitors FK866 or GMX1778 significantly reduced the NAD^+/NADH ratio and had no effect on the senescence-associated growth arrest as evidenced by no changes in decreased colony formation and markers of senescence such as Lamin B1 expression and senescence-associated beta-galactosidase (SA-β-Gal) activity (**Figure 1B-F**). Notably, NAMPT regulates the SASP in a NFκB dependent manner (21). Indeed, NFκB activity and SASP gene expression were significantly inhibited by treatment with the NAMPT inhibitors (**Figure 1G-H**). Similar observations were also made in additional EOC cell lines and in response to carboplatin (**Supplementary Figure 1A-F and Supplementary Figure 2A-D**), indicating that the observed effects are not cell-line specific. To limit the potential off-target effects of the NAMPT inhibitors, we generated a doxycycline (DOX)-inducible NAMPT knockdown system that significantly reduced the NAD^+/NADH ratio (**Figure 2A-B**). Consistently, DOX-inducible knockdown of NAMPT significantly reduced the SASP gene expression and did not affect senescence-associated growth arrest (**Figure 2C-F**). Conversely, we promoted the NAMPT pathway by

supplementing with the NAD^+ precursor nicotinamide mononucleotide (NMN) that significantly raised the NAD^+/NADH ratio (**Figure 2G**). Indeed, we found that NMN treatment significantly elevated SASP gene expression and did not affect senescence-associated growth arrest (**Figure 2H-K**). Thus, these data show that NAMPT has a role in promoting the SASP and functions independently of the senescence-associated growth arrest during platinum-induced senescence of EOC cells.

NAMPT promotes senescence-associated CSCs

Recent studies have shown that cellular senescence is a major contributor towards the increase of CSCs (11). We next sought to determine if NAMPT is required for the increase of CSCs following platinum-induced senescence. Following cisplatin treatment, we assessed outgrowth of EOC cells and markers of stemness. The NAMPT inhibitors significantly suppressed the outgrowth of EOC cells following cisplatin treatment using colony formation assays (**Figure 3A-B**). This correlated with suppression of upregulated ALDH1 protein level and *ALDH1A1* mRNA along with other stemness-related genes induced by cisplatin (**Figure 3C-E and Supplementary Figure 3A**). Indeed, the NAMPT inhibitors decreased the percentage of CD133 and ALDH-positive CSCs (**Figure 3F-G**). Notably, NAMPT inhibitors alone did not affect the growth of EOC cells at the doses used in the study (**Figure 3A-B**), indicating that they did not target the bulk non-stem cells. We also observed an increase in apoptotic markers, such as cleaved PARP and cleaved caspase 3, in the cells treated with the NAMPT inhibitors and cisplatin in combination compared with either treatment alone (**Figure 3C-D**). This is consistent with previous finding that suppressing ALDH activity induces apoptosis of EOC CSCs (28). Similar findings were also made in additional EOC cell lines (**Supplementary Figure 3B-E**).

We also examined if cisplatin treatment promotes CSCs in primary EOC specimens by developing an organoid-like three-dimensional system. Primary EOC specimens were processed and cultured in matrigel to form organoid-like structures as depicted using phase contrast and hematoxylin and eosin histological staining (**Figure 3H**). NAMPT inhibitor and cisplatin combination significantly reduced the diameter of organoid-like culture in comparison to the cisplatin alone-treated group (**Figure 3I**). More importantly, NAMPT inhibition significantly suppressed elevated ALDH activity induced by cisplatin treatment (**Figure 3J**). Finally, to limit the potential off-target effects, we examined the effects of DOX-inducible knockdown of NAMPT on the cisplatin-induced EOC CSCs. DOX-inducible knockdown of NAMPT significantly prevented the outgrowth of EOC cells following cisplatin treatment using colony formation assays (**Supplementary Figure 4A-B**). These results correlated with the suppression of ALDH1 protein level and *ALDH1A1* mRNA expression, stemness-related gene expression, and the increase of CD133 and ALDH-positive CSCs induced by cisplatin during senescence (**Supplementary Figure 4C-F**). Conversely, augmentation of the NAMPT pathway using NMN supplementation significantly promoted outgrowth, ALDH1 protein level and *ALDH1A* mRNA expression, and the increase of CD133 and ALDH-positive CSCs following cisplatin treatment (**Supplementary Figure 5A-E**). Together, these findings support the notion that NAMPT-regulated NAD^+ biogenesis pathway is both necessary and sufficient for therapy-induced senescence-associated CSCs.

We next sought to determine if senescent cells exhibit stemness following cisplatin treatment. To so do, we assessed cells for positivity for SA-β-Gal and ALDH activity using FACS analysis. We found cisplatin treatment significantly elevated senescent cells expressing high ALDH activity that was absent in the combinatorial cisplatin and NAMPT inhibitor-treated cells (**Figure 4A-B**). Given the fact that NAMPT inhibition does not affect senescence and the associated growth arrest, these findings suggest that the observed increase in senescent cells

with ALDH activity is due to the NAMPT-dependent SASP. Using fluorescence-based FACS sorting, we isolated the senescent CSC population and examined the effect of the NAMPT inhibitors on anchorage-independent sphere formation, a characteristic of putative ovarian CSCs (29). Notably, the NAMPT inhibitors suppressed sphere formation to a degree that is comparable with the ALDH-negatively sorted cells (**Figure 4C-D**). Conversely, promoting NAMPT pathway using NMN supplementation further promoted sphere formation (**Figure 4C-D**).

Since NAMPT plays a key role in the SASP, we next determined whether the observed changes in CSCs during therapy-induced senescence is SASP-dependent. Toward this goal, we determined if treatment of naïve EOC cells with conditioned media from cisplatin-induced senescent EOC cells in the presence or absence of the NAMPT inhibitors would affect the enrichment of CSCs (**Figure 5A**). We found that conditioned media from the cisplatin-induced senescent EOC cells significantly elevated the increase of CD133 and ALDH-positive CSCs and the expression of stemness-related genes. However, conditioned media collected from cisplatin-induced senescent EOC cells in the presence of the NAMPT inhibitors prevented the enrichment of the stemness signature (**Figure 5B-D**). Notably, the conditioned media did not induce senescence in these naïve EOC cells (**Supplementary Figure 6A-B**), indicating that the observed increase in CSCs by conditional medium was not a secondary effect due to senescence induction by conditional medium in these cells. These results suggest that the NAMPT-regulated SASP plays a key role in senescence-associated CSCs induced by cisplatin in EOC cells.

Combination of NAMPT inhibitor and cisplatin delays relapse and improves survival *in vivo*

NAMPT is highly expressed in several cancer types including EOC (30,31). We found through datamining of The Cancer Genome Atlas (TCGA) and gene expression datasets that

high NAMPT is significantly correlated with poorer overall survival of EOC patients and the expression of SASP factors (**Supplementary Figure 7A-B**) (27). Clinically applicable NAMPT inhibitors have been developed (30,32,33). Thus, we sought to determine the effects of NAMPT inhibitor on tumor relapse after cisplatin treatment. Toward this goal, we subcutaneously transplanted OVCAR3 cells into female immunocompromised non-obese diabetic/severe combined immunodeficiency gamma (NSG) mice. The injected cells were allowed to grow for four weeks to establish tumors. Then, we randomly assigned the mice into four groups and treated mice with vehicle control, cisplatin (750 μg/kg every two weeks), FK866 (10 mg/kg daily), or a combination of cisplatin and FK866 by intraperitoneal injection for an additional three weeks (**Figure 6** and **Supplementary Figure 8A**).

After three weeks of treatment, we harvested the tumors and found that the tumor growth or weight was not significantly reduced by FK866 alone treatment but was significantly lower in the cisplatin-treated groups (**Figure 6A-B** and **Supplementary Figure 8B**). Notably, the combination did not significantly further reduce the tumor weight compared to cisplatin treatment group at the time of stopping treatment (**Figure 6B**). We examined ALDH activity and found ALDH activity was elevated in the cisplatin-treated group, while significantly decreased in the combination cisplatin and FK866 group (**Figure 6C** and **Supplementary Figure 8C**). Consistent with this result, we found that the combination cisplatin and FK866 group had significantly lower ALDH1 protein and *ALDH1A1* mRNA expression compared to the cisplatin-treated group (**Figure 6D-F**). Consistent with *in vitro* findings, we showed that markers of senescence such as SA-β-Gal activity induced by cisplatin was not significantly affected by FK866 *in vivo* in the harvested tumors (**Supplementary Figure 8C-D**). Notably, combination of cisplatin and FK866 significantly reduced the expression of SASP factors such as *IL6* (**Supplementary Figure 8E**). We next followed the tumor outgrowth in mice treated with cisplatin with or without FK866 combination after terminating drug treatment. We found the

outgrowth of the tumors in the combination treatment group was significantly slower compared with the cisplatin only treatment group (**Figure 6G**). Indeed, the survival of the combination-treated mice was also significantly extended compared with mice treated with cisplatin alone (**Figure 6H**). Notably, the combination of cisplatin and FK866 did not exhibit toxicity in the treated mice. For example, the body weight of the treated mice was not significantly affected by the combination treatment (**Supplementary Figure 8F**). Taken together, we conclude that a combination of FK866 and cisplatin improves the survival of EOC-bearing mice, which correlated with the suppression of senescence-associated CSCs.

Discussion

Our results suggest that HMGA1 drives NAMPT expression to promote CSCs following platinum-based chemotherapy. Consistently, it has been demonstrated that HMGA1 is often upregulated in a range of human cancers and associated with a poorer patient prognosis (34). Interestingly, HMGA1 is enriched in intestinal stem cells and enhances self-renewal and expands the intestinal stem cells compartment (35). In addition, HMGA1 is required for progression and stem cell properties in multiple cancer types including colorectal cancer (36). However, it is difficult to target chromatin architecture proteins such as HMGA1. Thus, our present study suggests that NAMPT inhibitors may be used in HMGA1-high cancers to suppress cancer stem-like cells.

We found that elevated NAD^+ level was associated with activation of NFκB signaling and the SASP during therapy-induced senescence. Consistently, it has previously been shown that IL6, a component of the SASP, is a key regulator of stemness in response to platinum-based chemotherapy in EOC (37). Notably, supplementation with the NAD^+ precursor NMN to enhance the NAMPT pathway promotes CSCs following platinum-based chemotherapy. Thus, NAD^+-augmenting dietary supplements, which have been clinically tested to alleviate age-related pathophysiological conditions, may have unintended side-effects of promoting CSCs (38,39). Therefore, further studies are warranted in this area of research.

Our studies demonstrate that targeting NAMPT activity through the use of clinically applicable NAMPT inhibitors represents a novel strategy for targeting senescence-associated CSCs in EOC. Similar results were obtained by using two different NAMPT inhibitors FK866 and GMX1778. The potential off-target effects of the NAMPT inhibitors were further limited by phenocopying with genetically knocking down NAMPT expression. Together, these findings

support that the observed effects by FK866 are on-target through inhibiting NAMPT activity. Addition of NAMPT inhibitor significantly delayed tumor relapse and improved survival of EOC-bearing mice *in vivo* compared with cisplatin treatment alone. Notably, the dose of NAMPT inhibitor used in the current study did not significantly affect the tumor growth when used as a single agent. This is consistent with the idea that NAMPT inhibition suppresses the CSCs induced by platinum-based chemotherapy instead of targeting bulk tumor cells in this context. Together, our study indicates that NAMPT inhibitors may be repurposed to suppress therapy-induced senescence-associated CSCs for improving platinum-based standard of care, a major obstacle in the clinical management of EOC.

Acknowledgements

This work was supported by US National Institutes of Health grants (R01CA160331, R01CA163377, R01CA202919, R01CA239128, P01AG031862 and P50CA228991 to R. Z., and T32CA009191 to T.N.) and US Department of Defense (OC150446 and OC180109 to R. Z.). The Honorable Tina Brozman Foundation for Ovarian Cancer Research (to R.Z.) and Ovarian Cancer Research Alliance (Collaborative Research Development Grant to R.Z.). Support of Core Facilities was provided by Cancer Centre Support Grant (CCSG) CA010815 to The Wistar Institute.

References

1. Kurman RJ, Shih Ie M. The Dualistic Model of Ovarian Carcinogenesis: Revisited, Revised, and Expanded. Am J Pathol **2016**;186:733-47
2. Bowtell DD, Bohm S, Ahmed AA, Aspuria PJ, Bast RC, Jr., Beral V*, et al.* Rethinking ovarian cancer II: reducing mortality from high-grade serous ovarian cancer. Nat Rev Cancer **2015**;15:668-79
3. Zhang S, Balch C, Chan MW, Lai HC, Matei D, Schilder JM*, et al.* Identification and characterization of ovarian cancer-initiating cells from primary human tumors. Cancer Res **2008**;68:4311-20
4. Silva IA, Bai S, McLean K, Yang K, Griffith K, Thomas D*, et al.* Aldehyde dehydrogenase in combination with CD133 defines angiogenic ovarian cancer stem cells that portend poor patient survival. Cancer Res **2011**;71:3991-4001
5. Deng S, Yang X, Lassus H, Liang S, Kaur S, Ye Q*, et al.* Distinct expression levels and patterns of stem cell marker, aldehyde dehydrogenase isoform 1 (ALDH1), in human epithelial cancers. PLoS One **2010**;5:e10277
6. Zhang J, Guo X, Chang DY, Rosen DG, Mercado-Uribe I, Liu J. CD133 expression associated with poor prognosis in ovarian cancer. Mod Pathol **2012**;25:456-64
7. Landen CN, Jr., Goodman B, Katre AA, Steg AD, Nick AM, Stone RL*, et al.* Targeting aldehyde dehydrogenase cancer stem cells in ovarian cancer. Mol Cancer Ther **2010**;9:3186-99
8. Flesken-Nikitin A, Hwang CI, Cheng CY, Michurina TV, Enikolopov G, Nikitin AY. Ovarian surface epithelium at the junction area contains a cancer-prone stem cell niche. Nature **2013**;495:241-5

9. Lissanu Deribe Y, Sun Y, Terranova C, Khan F, Martinez-Ledesma J, Gay J*, et al.* Mutations in the SWI/SNF complex induce a targetable dependence on oxidative phosphorylation in lung cancer. Nat Med **2018**;24:1047-57

10. Campisi J. Aging, cellular senescence, and cancer. Annu Rev Physiol **2013**;75:685-705

11. Milanovic M, Fan DNY, Belenki D, Dabritz JHM, Zhao Z, Yu Y*, et al.* Senescence-associated reprogramming promotes cancer stemness. Nature **2018**;553:96-100

12. Coppe JP, Desprez PY, Krtolica A, Campisi J. The senescence-associated secretory phenotype: the dark side of tumor suppression. Annu Rev Pathol **2010**;5:99-118

13. Munoz-Galvan S, Lucena-Cacace A, Perez M, Otero-Albiol D, Gomez-Cambronero J, Carnero A. Tumor cell-secreted PLD increases tumor stemness by senescence-mediated communication with microenvironment. Oncogene **2019**;38:1309-23

14. Milanovic M, Yu Y, Schmitt CA. The Senescence-Stemness Alliance - A Cancer-Hijacked Regeneration Principle. Trends Cell Biol **2018**;28:1049-61

15. Demaria M, O'Leary MN, Chang J, Shao L, Liu S, Alimirah F*, et al.* Cellular Senescence Promotes Adverse Effects of Chemotherapy and Cancer Relapse. Cancer Discov **2017**;7:165-76

16. Canto C, Menzies KJ, Auwerx J. NAD(+) Metabolism and the Control of Energy Homeostasis: A Balancing Act between Mitochondria and the Nucleus. Cell Metab **2015**;22:31-53

17. Garten A, Schuster S, Penke M, Gorski T, de Giorgis T, Kiess W. Physiological and pathophysiological roles of NAMPT and NAD metabolism. Nat Rev Endocrinol **2015**;11:535-46

18. Yoshino J, Baur JA, Imai SI. NAD(+) Intermediates: The Biology and Therapeutic Potential of NMN and NR. Cell Metab **2018**;27:513-28

19. Yaku K, Okabe K, Hikosaka K, Nakagawa T. NAD Metabolism in Cancer Therapeutics. Front Oncol **2018**;8:622

20. Audrito V, Manago A, Gaudino F, Sorci L, Messana VG, Raffaelli N*, et al.* NAD-Biosynthetic and Consuming Enzymes as Central Players of Metabolic Regulation of Innate and Adaptive Immune Responses in Cancer. Front Immunol **2019**;10:1720

21. Nacarelli T, Lau L, Fukumoto T, Zundell J, Fatkhutdinov N, Wu S*, et al.* NAD(+) metabolism governs the proinflammatory senescence-associated secretome. Nat Cell Biol **2019**;21:397-407

22. Fukumoto T, Zhu H, Nacarelli T, Karakashev S, Fatkhutdinov N, Wu S*, et al.* N(6)-Methylation of Adenosine of FZD10 mRNA Contributes to PARP Inhibitor Resistance. Cancer Res **2019**;79:2812-20

23. Yokoyama Y, Zhu H, Lee JH, Kossenkov AV, Wu SY, Wickramasinghe JM*, et al.* BET Inhibitors Suppress ALDH Activity by Targeting ALDH1A1 Super-Enhancer in Ovarian Cancer. Cancer Res **2016**;76:6320-30

24. Piacente F, Caffa I, Ravera S, Sociali G, Passalacqua M, Vellone VG*, et al.* Nicotinic Acid Phosphoribosyltransferase Regulates Cancer Cell Metabolism, Susceptibility to NAMPT Inhibitors, and DNA Repair. Cancer Res **2017**;77:3857-69

25. Sociali G, Raffaghello L, Magnone M, Zamporlini F, Emionite L, Sturla L*, et al.* Antitumor effect of combined NAMPT and CD73 inhibition in an ovarian cancer model. Oncotarget **2016**;7:2968-84

26. Tang Z, Li C, Kang B, Gao G, Li C, Zhang Z. GEPIA: a web server for cancer and normal gene expression profiling and interactive analyses. Nucleic Acids Res **2017**;45:W98-W102

27. Tothill RW, Tinker AV, George J, Brown R, Fox SB, Lade S*, et al.* Novel molecular subtypes of serous and endometrioid ovarian cancer linked to clinical outcome. Clin Cancer Res **2008**;14:5198-208

28. Zhu H, Bengsch F, Svoronos N, Rutkowski MR, Bitler BG, Allegrezza MJ*, et al.* BET Bromodomain Inhibition Promotes Anti-tumor Immunity by Suppressing PD-L1 Expression. Cell Rep **2016**;16:2829-37

29. Wang Y, Cardenas H, Fang F, Condello S, Taverna P, Segar M*, et al.* Epigenetic targeting of ovarian cancer stem cells. Cancer Res **2014**;74:4922-36

30. Tan B, Young DA, Lu ZH, Wang T, Meier TI, Shepard RL*, et al.* Pharmacological inhibition of nicotinamide phosphoribosyltransferase (NAMPT), an enzyme essential for NAD+ biosynthesis, in human cancer cells: metabolic basis and potential clinical implications. J Biol Chem **2013**;288:3500-11

31. Shackelford RE, Bui MM, Coppola D, Hakam A. Over-expression of nicotinamide phosphoribosyltransferase in ovarian cancers. Int J Clin Exp Pathol **2010**;3:522-7

32. Roulston A, Shore GC. New strategies to maximize therapeutic opportunities for NAMPT inhibitors in oncology. Mol Cell Oncol **2016**;3:e1052180

33. Sampath D, Zabka TS, Misner DL, O'Brien T, Dragovich PS. Inhibition of nicotinamide phosphoribosyltransferase (NAMPT) as a therapeutic strategy in cancer. Pharmacol Ther **2015**;151:16-31

34. Sumter TF, Xian L, Huso T, Koo M, Chang YT, Almasri TN*, et al.* The High Mobility Group A1 (HMGA1) Transcriptome in Cancer and Development. Curr Mol Med **2016**;16:353-93

35. Xian L, Georgess D, Huso T, Cope L, Belton A, Chang YT*, et al.* HMGA1 amplifies Wnt signalling and expands the intestinal stem cell compartment and Paneth cell niche. Nat Commun **2017**;8:15008

36. Belton A, Gabrovsky A, Bae YK, Reeves R, Iacobuzio-Donahue C, Huso DL*, et al.* HMGA1 induces intestinal polyposis in transgenic mice and drives tumor progression and stem cell properties in colon cancer cells. PLoS One **2012**;7:e30034

37. Wang Y, Zong X, Mitra S, Mitra AK, Matei D, Nephew KP. IL-6 mediates platinum-induced enrichment of ovarian cancer stem cells. JCI Insight **2018**;3

38. Verdin E. NAD(+) in aging, metabolism, and neurodegeneration. Science **2015**;350:1208-13

39. Canto C, Houtkooper RH, Pirinen E, Youn DY, Oosterveer MH, Cen Y*, et al.* The NAD(+) precursor nicotinamide riboside enhances oxidative metabolism and protects against high-fat diet-induced obesity. Cell Metab **2012**;15:838-47

Figure Legends

Figure 1. NAMPT inhibition suppresses cisplatin-induced SASP.

(**A**) OVCAR3 cells treated with or without 250 nM cisplatin for four days were subjected to ChIP analysis for the enrichment of HMGA1 on the *NAMPT* gene enhancer using an anti-HMGA1 antibody or isotype-match IgG control. (**B**) OVCAR3 cells treated with cisplatin with or without 1 nM FK866 or 0.5 nM GMX1778 for four days were examined for the expression of HMGA1, NAMPT, Lamin B1, and a loading control β-actin by immunoblotting. (**C**) Same as (B), but cells were examined for the NAD^+/NADH ratio. (**D**) Cells treated under the indicated conditions were examined for SA-β-Gal activity or colony formation at day 5 with the indicated treatment. Scale bar = 100 μm. (**E**) Quantification of SA-β-Gal positive cells in (D). (**F**) Quantification of integrated intensity of colony formation in (D). (**G**) Cells under the indicated conditions were assayed for NFκB reporter activity. (**H**) Same as in (B), but cells were examined for SASP gene expression using qRT-PCR. Note that high cell density was used for SA-β-Gal assay to avoid stress-induced false positivity, while low cell density was used for colony formation to examine the differences in cell proliferation. Error bars represent ± S.E.M. n = 3 independent experiments. *P* values were calculated using a two-tailed Student's *t*-test.

Figure 2. NAD^+ level regulates cisplatin-induced SASP.

(**A**) OVCAR3 cells treated with cisplatin with or without DOX-inducible knockdown of NAMPT for four days were examined for expression of NAMPT, Lamin B1, and a loading control β-actin by immunoblot. (**B**) Same as (A), but cells were examined for the NAD^+/NADH ratio. (**C**) Same as (A), but cells were examined for the indicated SASP gene expression using qRT-PCR. (**D**) Cells treated under the indicated conditions were examined for SA-β-Gal activity or colony formation. Scale bar = 100 μm. (**E**) Quantification of SA-β-Gal positive cells in (D). (**F**) Quantification of

integrated intensity of colony formation in (D). (**G**) Cells treated with cisplatin with or without 500 μM NMN supplementation were examined for the NAD^+/NADH ratio. (**H**) Same as in (G), but cells were examined for the indicated SASP gene expression using qRT-PCR. (**I**) Cells treated under the indicated conditions were examined for SA-β-Gal activity or colony formation. Scale bar = 100 μm. (**J**) Quantification of SA-β-Gal positive cells in (I). (**K**) Quantification of integrated intensity of colony formation in (I). Error bars represent ± S.E.M. n = 3 independent experiments. *P* values were calculated using a two-tailed Student's *t*-test.

Figure 3. NAMPT inhibition suppresses therapy-induced CSCs.

(**A**) OVCAR3 cells were treated with 250 nM cisplatin with or without 1 nM FK866 or 0.5 nM GMX1778 and released from treatment and further cultured in drug-free medium for 9 days and assayed for colony formation. (**B**) Quantification of integrated intensity of colony formation in (A). (**C-D**) Same as in (A), but cells were only treated for four days and examined for expression of ALDH1A1, NAMPT, Cleaved PARP1, Cleaved Caspase 3, and a loading β-actin by immunoblot. (**E**) Same as in (C), but cells were analyzed for expression of the indicated stem-related genes by qRT-PCR. (**F**) Same as in (C), but cells were analyzed for ALDH activity and CD133 positivity by FACS. (**G**) Quantification of the percentage of ALDH and CD133-positive cells in (F). DEAB-treated cells were used as a negative control for ALDH activity. Error bars represent ± S.E.M. n = 3 independent experiments. (**H**) Primary EOC cells were harvested from a serous EOC histosubtype tumor specimen, grown into organoid structures under three-dimensional conditions, and subjected to phase contract microscopy and hematoxylin–eosin (H&E) staining. Scale bar for phase contrast = 100 μm. Scale bar for H&E staining = 40 μm. (**I**) Organoid structures were treated with 250 nM cisplatin with or without 1 nM FK866 and examined for organoid diameter. Organoids larger than 40 μm were quantified. (**J**) Same as in (I), but cells were stained for ALDH activity and imaged on a Celígo imaging cytometer. Error bars represent

± S.E.M. n = 2 independent experiments. *P* values were calculated using a two-tailed Student's *t*-test.

Figure 4. NAMPT inhibitors suppress senescence-associated EOC CSCs.

(**A**) OVCAR3 cells were treated with 250 nM cisplatin with or without 1 nM FK866 or 0.5 nM GMX1778 and analyzed for ALDH and SA-β-Gal activity by FACS. (**B**) Quantification of the percentage of ALDH and SA-β-Gal-positive cells in (A). (**C**) FACS-sorted ALDH and SA-β-Gal-positive cells were cultured in low attachment plates to assess sphere formation with or without 1 nM FK866, 0.5 nM GMX1778, or 500 μM NMN treatment. Scale bar = 100 μm. (**D**) Quantification of sphere formation in (C). Error bars represent ± S.E.M. n = 3 independent experiments. *P* values were calculated using a two-tailed Student's *t*-test.

Figure 5. NAMPT-driven SASP promotes stemness.

(**A**) Schematic of experimental design. OVCAR3 cells were treated with 250 nM cisplatin with or without 1 nM FK866 or 0.5 nM GMX1778 and released from treatment for the collection of conditioned media. Naïve OVCAR3 cells were treated with conditioned media and assayed for stemness markers. (**B**) Cells were analyzed for ALDH activity and CD133 positivity by FACS. (**C**) Quantification of the percentage of ALDH and CD133-positive cells in (B). (**D**) Same as in (A), but cells were analyzed for expression of the indicated stem-related genes by qRT-PCR. Error bars represent ± S.E.M. n = 3 independent experiments. *P* values were calculated using a two-tailed Student's *t*-test.

Figure 6. The combination of FK866 and cisplatin suppresses tumor outgrowth and improves survival of EOC-bearing mice. (**A**) The growth of tumors formed by OVCAR3 cells

in the indicated treatment groups (n=6 mice/group) was monitored at the indicated time points during the three weeks of treatment. (**B**) After three weeks of treatment, the mice from the indicated treatment groups were euthanized and the weights of the dissected tumors were quantified as a surrogate for tumor burden (n=4 mice/group). (**C**) Tumors from in (B) were examined for ALDH activity by FACS (n=4 mice/group). (**D**) Tumors from in (B) were examined for *ALDH1A1* expression by qRT-PCR (n=4 mice/group). (**E**) The tumor tissue sections from the indicated treatment groups were subjected to hematoxylin–eosin (H&E) staining and immunohistochemical staining using an antibody against ALDH1. Scale bar = 100 μm. (**F**) The histological score (H-score) of ALDH1 was calculated from (E) (n=4 mice/group). (**G**) Quantification of tumor outgrowth in the indicated groups after terminating drug treatment (n=6 mice/group). (**H**) After three weeks of treatment of cisplatin with or without FK866, the mice were followed for survival and shown are the Kaplan-Meier survival curves (n=6 mice/group). Error bars represent ± S.E.M. *P* values were calculated using a two-tailed Student's *t*-test.

Author Manuscript Published OnlineFirst on December 19, 2019; DOI: 10.1158/0008-5472.CAN-19-2830
Author manuscripts have been peer reviewed and accepted for publication but have not yet been edited.

Figure 1

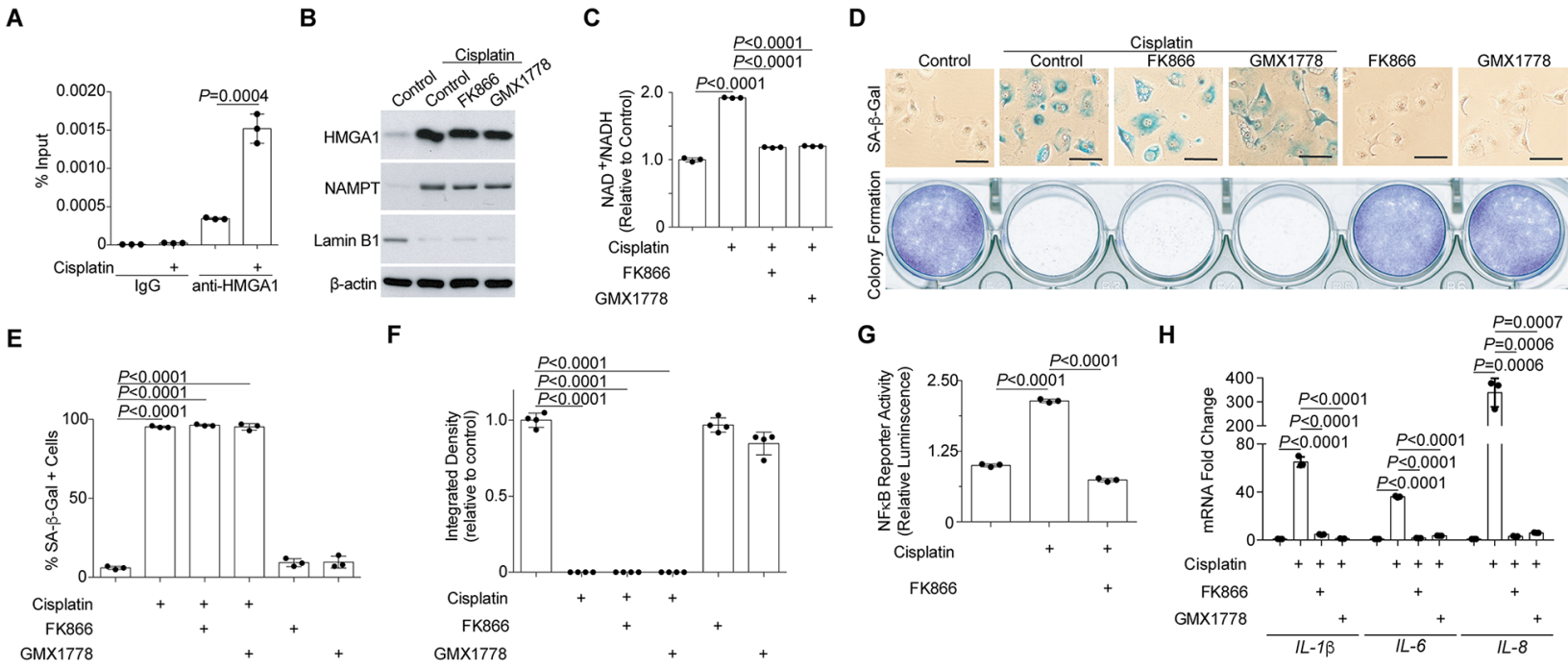

Author Manuscript Published OnlineFirst on December 19, 2019; DOI: 10.1158/0008-5472.CAN-19-2830
Author manuscripts have been peer reviewed and accepted for publication but have not yet been edited.

Figure 2

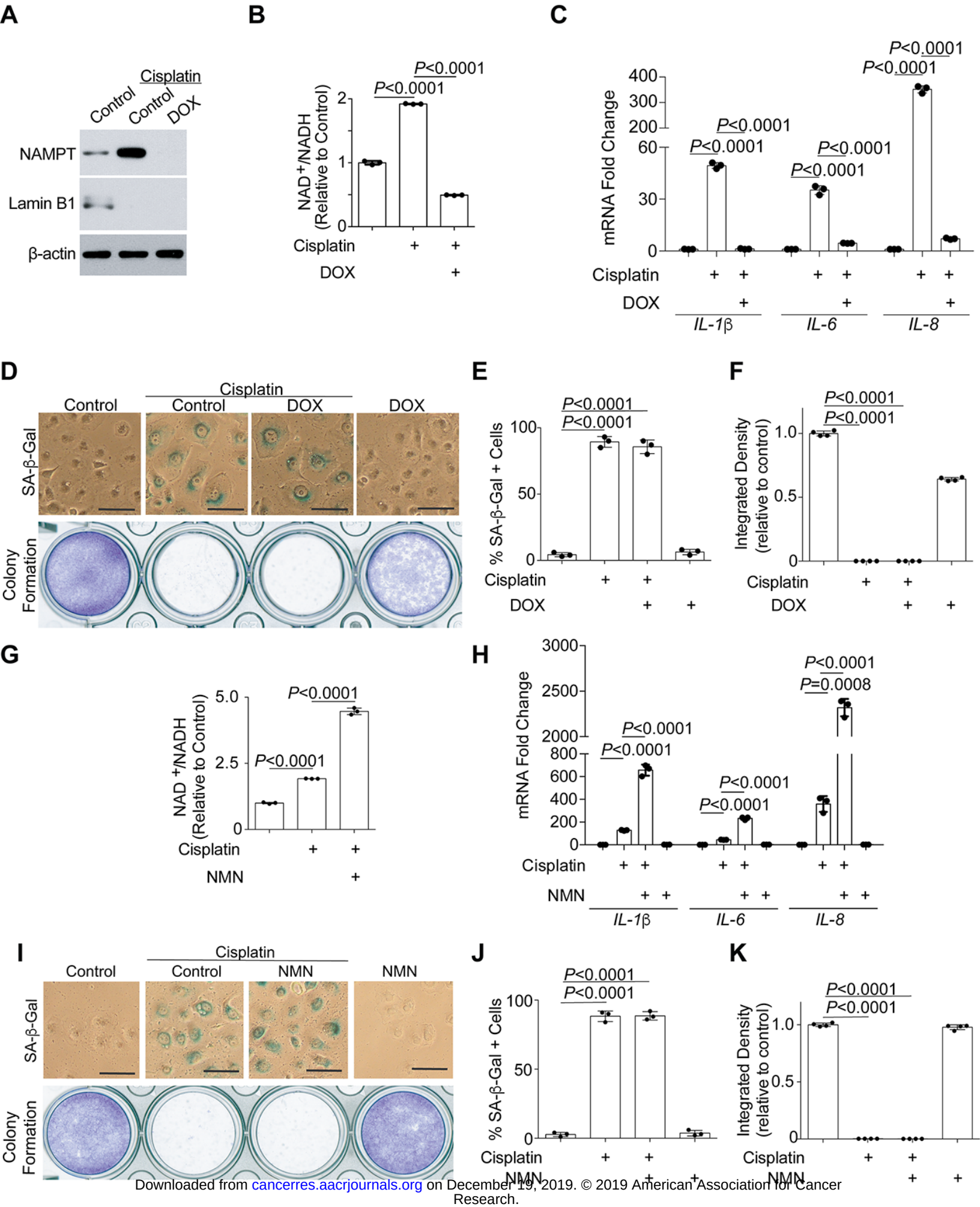

Figure 3

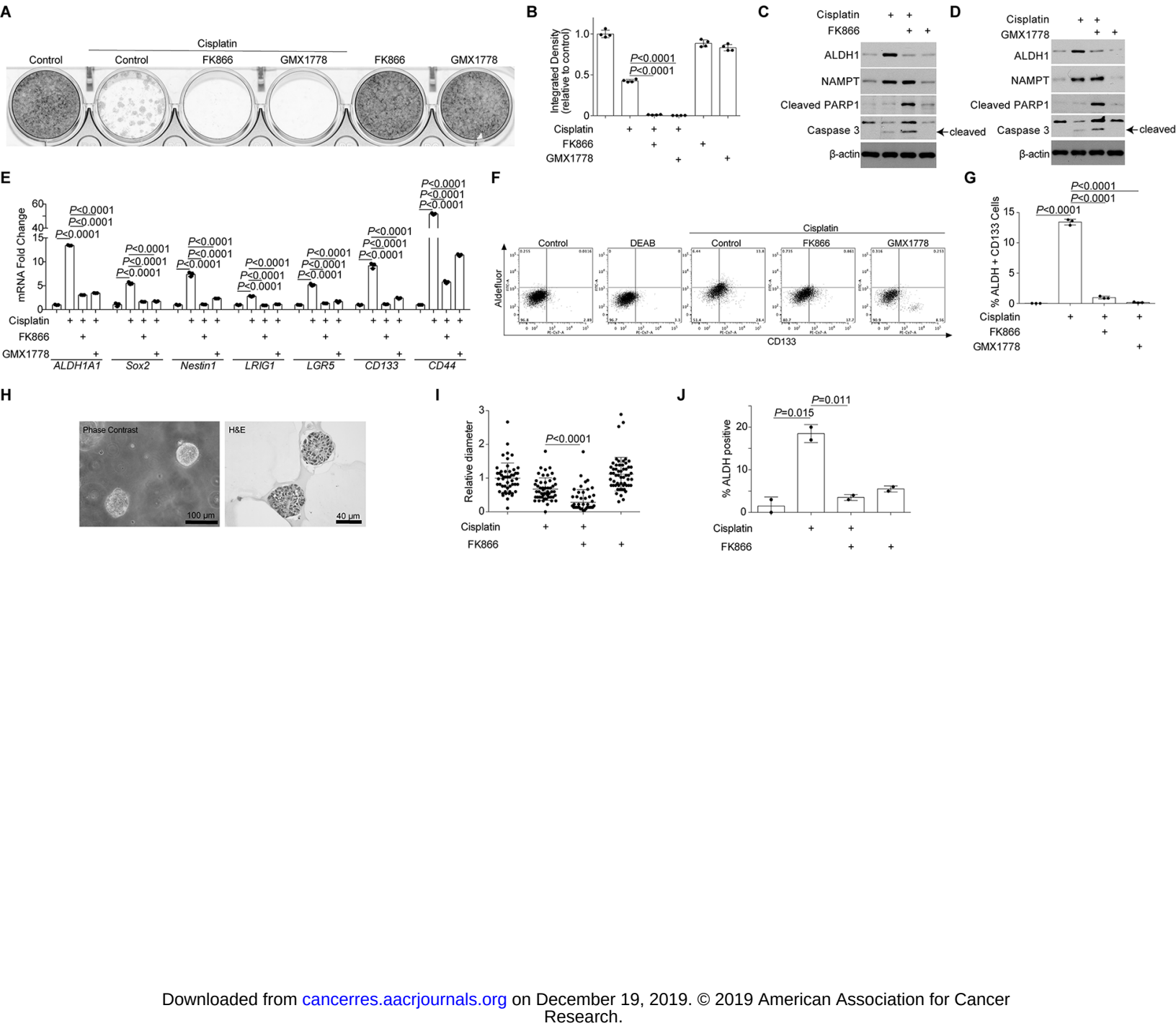

Author Manuscript Published OnlineFirst on December 19, 2019; DOI: 10.1158/0008-5472.CAN-19-2830
Author manuscripts have been peer reviewed and accepted for publication but have not yet been edited.

Figure 4

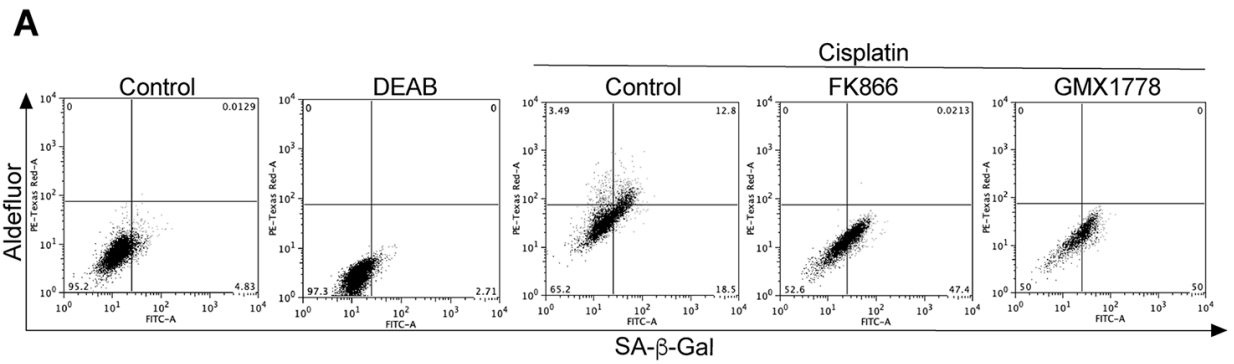

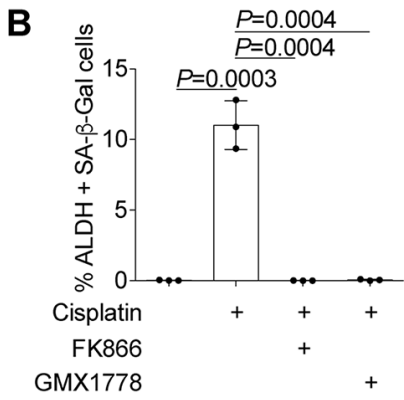

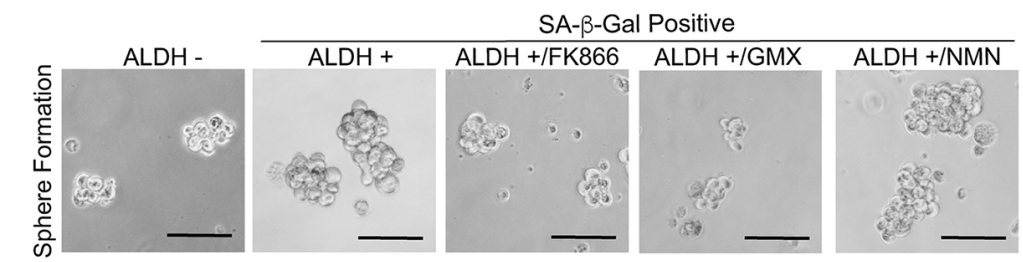

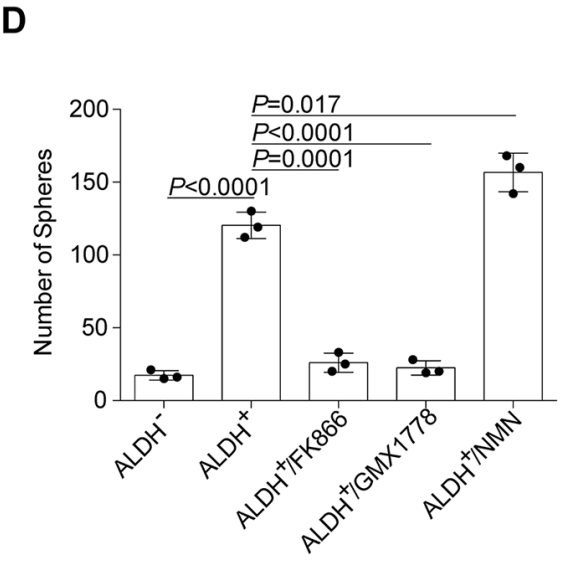

Figure 5

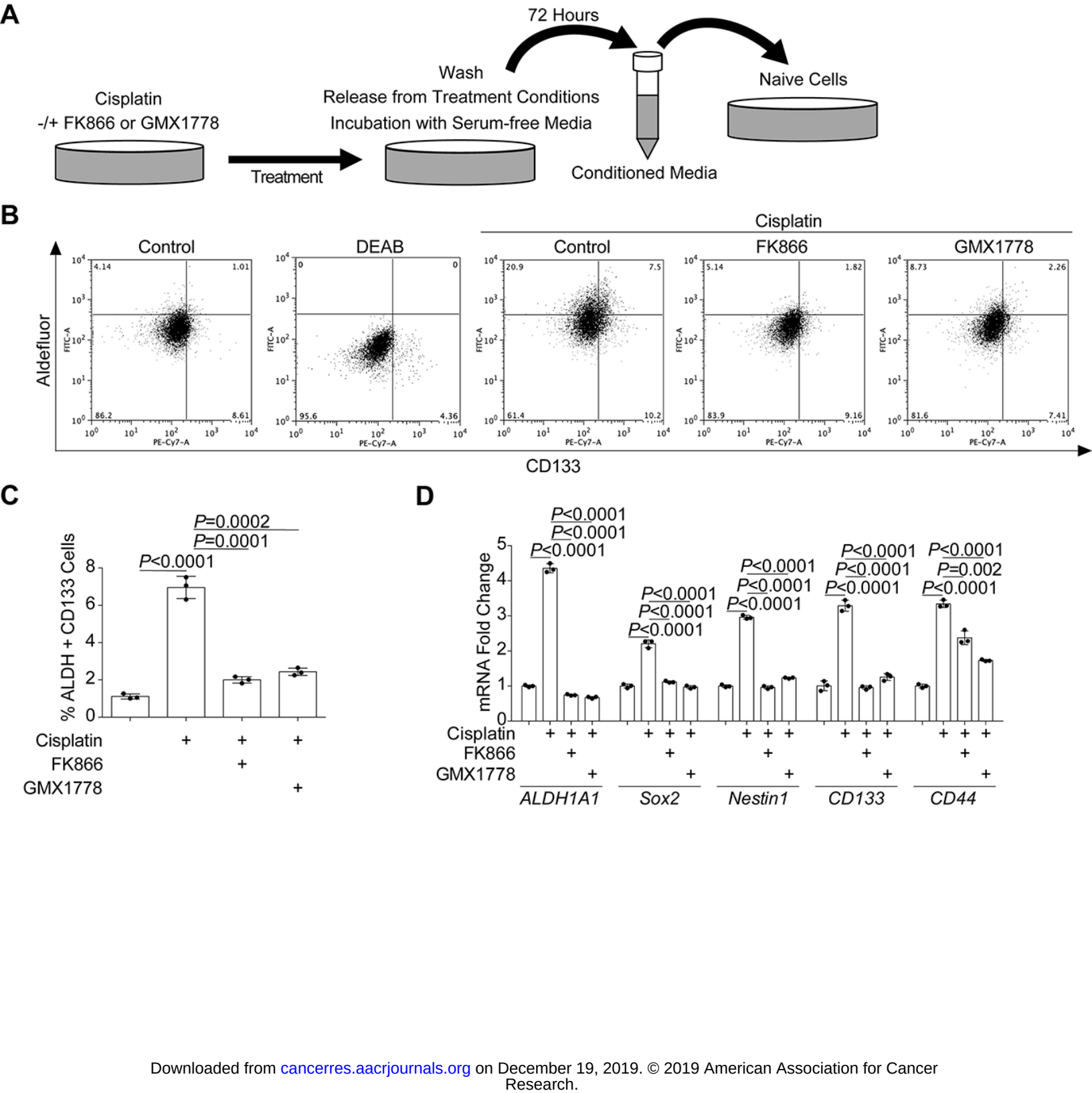

Figure 6

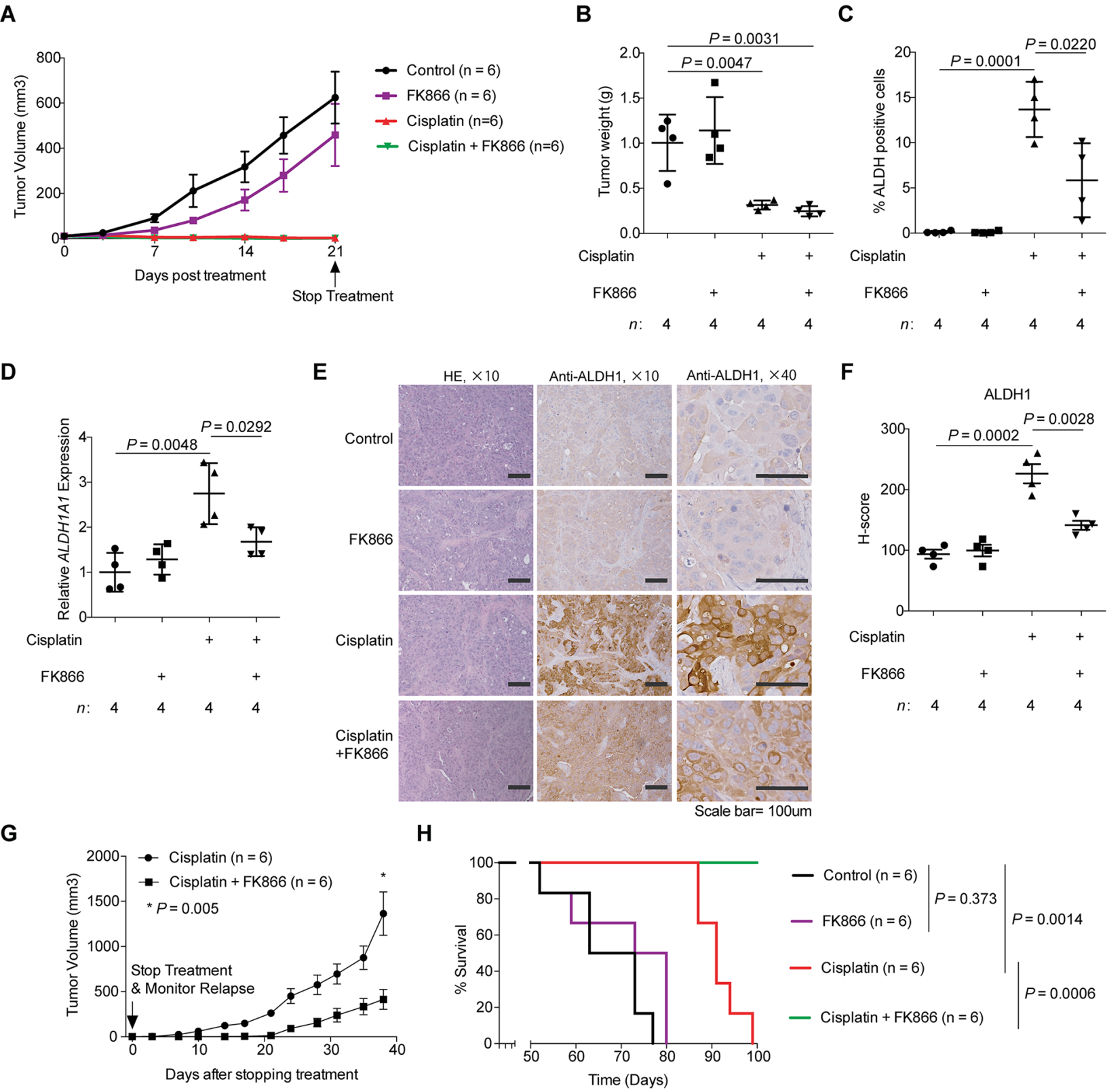

AACR American Association for Cancer Research

Cancer Research

The Journal of Cancer Research (1916–1930) | The American Journal of Cancer (1931–1940)

NAMPT inhibition suppresses cancer stem-like cells associated with therapy-induced senescence in ovarian cancer

Timothy Nacarelli, Takeshi Fukumoto, Joseph A. Zundell, et al.

Cancer Res Published OnlineFirst December 19, 2019.